Mechanics Research Communications 134 (2023) 104212

Contents lists available at ScienceDirect

Mechanics Research Communications

journal homepage: www.elsevier.com/locate/mechrescom

Thermo-mechanical experimental investigations of 3D-printed elastomeric polyurethane from low to intermediate strain rates

Jie Yang [a,b], Zisheng Liao [a,b], Mokarram Hossain [b,*], Guanyu Huang [a], Kai Wang [a], Xiaohu Yao [a]

[a] State Key Laboratory of Subtropical Building Science, South China University of Technology, Guangzhou 510640, China
[b] Zienkiewicz Institute for Modelling, Data and AI, Faculty of Science and Engineering, Swansea University, SA1 8EN, UK

ARTICLE INFO

Keywords:
Digitally-printed polyurethane
Experimental characterisation
Glass transition
Thermal sensitivity
Strain rate sensitivity

ABSTRACT

Additively manufactured (3D-printed) elastomers have increasing applications in impact resistance devices such as helmets, shoe soles, and shock absorbing architectured metamaterials. These rapidly expanding areas require a proper understanding of the thermo-mechanical behaviours of soft polymers. In this contribution, thermal–mechanical properties of 3D-printed elastomeric polyurethane (EPU) are extensively characterised under low to high strain rates which are missing in the literature. The EPU under investigation is digitally manufactured using a Digital Light Synthesis (DLS) technology and is characterised by tensile experiments with a wide range of strain rates spanning from 0.001/s to 500/s and temperature variations of -20 °C to 60 °C. The experimental results reveal deformation nonlinearity, thermal-sensitivity, and strain rate-sensitivity in the elastomer. Moreover, the study reveals the occurrence of the glass transition phenomenon, which is commonly observed in soft materials under low-temperature and high strain-rate conditions. Various graphical illustrations are presented to depict the effects of temperature and strain rate on the stress response. It is observed that as temperature decreases or strain rate increases, the stress amplifies and becomes more sensitive to variations in temperature or strain rate. Additionally, higher strain levels further enhance the stress sensitivity to these variations. The microscopic mechanisms behind the thermal and strain rate sensitivities are discussed, taking into account the influence of the strain level. Overall, this study contributes to a proper understanding of the thermo-mechanical behaviours of digitally-printed soft polymers, particularly in dynamic scenarios.

1. Introduction

Additive manufacturing (AM) technology, widely applied in aerospace [1,2], sports equipment [3,4], healthcare [1–9], and architecture [2,10], is celebrated for rapid prototyping, waste reduction, precision, and design flexibility [11]. Unlike traditional subtractive manufacturing, AM technology adds raw material, typically powder or liquid, layer-by-layer or dot-by-dot to build objects. Moreover, recent developments in 4D printing have further propelled AM technology into the realm of intelligent materials manufacturing [12–14]. This technology enables users to optimise the mechanical properties by adjusting printing parameters (e.g., tensile strength and impact resistance) of printedobjects [3,4,11,15–26], making AM technology ideal for producing personalised medical instruments, footwear, and protective gear, tailored to individual anatomical features.

Elastomeric polyurethane (EPU) has gained popularity across various engineering disciplines, including automotive manufacturing, construction, and sports equipment, primarily due to its excellent tear strength, low wave speeds, and exceptional impact resistance [10,27–32]. Numerous experimental investigations have provided valuable insights into the material's unique characteristics such as nonlinear deformation, strain rate dependence, hysteresis, and stress softening [33–36]. Given the critical applications of EPU in impact protection, it often encounters extreme circumstances, including low temperatures and high strain rates. Understanding its thermo-mechanical properties is crucial in such scenarios. Numerous experiments [37–47] have been conducted to investigate compression experiments from 10^{-3}/s to 10^{4}/s by using the split Hopkinson pressure bar technique. These experiments involved various soft materials, including polyurea, EPU, pig skin, and hydroxyl-terminated polybutadiene. A common observation across these studies is the strain rate sensitivity of soft materials, with an increase in stiffness and strength at higher strain rates. Furthermore, soft materials have been extensively explored for enhancing the ballistic and blast resistance of coated materials [10,30,48]. Moreover, the influence of temperature and strain-rate on tensile behaviour have been

* Corresponding author.
E-mail addresses: ctjyang@mail.scut.edu.cn (J. Yang), lzsheng2006@gmail.com (Z. Liao), mokarram.hossain@swansea.ac.uk (M. Hossain), ctgyhuang@mail.scut.edu.cn (G. Huang), chinawangkai96@hotmail.com (K. Wang), yaoxh@scut.edu.cn (X. Yao).

https://doi.org/10.1016/j.mechrescom.2023.104212
Received 25 May 2023; Received in revised form 12 October 2023; Accepted 21 October 2023
Available online 30 October 2023

examined [49,50]. Zhang et al. [51] and Liao et al. [32] conducted systematic experiments on the transparent EPU from −40 °C to 50 °C and 10^0/s to 10^3/s, revealing the impacts of temperature and strain rate changes on mechanical characteristics.

The aforementioned studies are important for understanding the behaviours of soft materials under extreme conditions. They reveal that soft polymers undergo a transition from a rubbery state to a glassy state with decreasing temperature and/or increasing strain rate, a phenomenon known as the glass transition [32,52–54]. A comprehensive understanding of this transition is crucial for designing novel materials and structures that can better withstand impacts and protect against injuries in applications like sports equipment and personal protective gear. Furthermore, the classical Time–Temperature Superposition (TTS) principle [55] has been widely adopted to elucidate the glass transition phenomenon and its correlation between temperature reduction and strain rate increase on the mechanical properties of soft materials, enabling the prediction of the mechanical behaviour over a wide range of strain rates [32,51,56].

However, the aforementioned dynamic experiments exclusively focused on conventionally manufactured soft materials such as injection moulding. While EPU has demonstrated its value in various fields, especially in dynamic scenarios, its potential in AM technology is yet to be fully explored. To the best of the authors' knowledge, there is currently no systematic investigation of the dynamic mechanical characteristics of digitally printed soft polymer materials. Considering the superior impact performance of EPU and the inherent advantages of AM technology, this study aims to bridge the existing gap of experimental studies on 3D printed soft polymers, which will contribute to improving engineering practices, such as quantifying external loads acting on structures in engineering settings [57]. In this case, the thermo-mechanical behaviours of digitally-printed EPU across a broad range of temperatures and strain rates that go through the glass transition have been investigated. This investigation contributes to the comprehension of material selection and structural optimisation for impact protective devices using 3D printed EPU.

The structure of this contribution is organised as follows. Apart from the current section, Section 2 specifies the details of the experimental setup. Further, the experimental results and discussion are specified in Section 3. Finally, the key contribution of the study is summarised in Section 4.

2. Experimental setup

The test specimens were prepared using Digital Light Synthesis (DLS) printing technique [1,2,58–60], which enables continuous construction and promotes the rapid prototyping and structural integration. For this vat-polymerisation process, the polymer layer is printed holistically, where UV light is projected across the entire layer to induce material curing through an oxygen-permeable window. Positioned between this window and the printing part, a slender layer composed of uncured resin forms what is termed the dead-zone, which is used to prevent adhesion between the printed part and the uncured resin, and to facilitate a continuous flow of liquid resins beneath the printed component. For more information about the printing details, see [36,58,59].

As indicated in [61,62], no discernible correlation has been observed between the printing angle and the mechanical characteristics of the samples printed using vat photopolymerisation techniques. Given that the focus of this contribution does not lie in the realm of printing conditions, we assume the isotropy of the DLS-based EPU for simplicity. Two types of dogbone-shaped specimens are used in our tests (see Fig. 1) due to the different clamping methods and different travel limits of the machine used in our experiments, as highlighted in Figs. 2(a) and 2(b). According to some initial trial experiments, the specimens were designed to ensure non-slippage and the prevention of fractures near the clip position by the following actions:

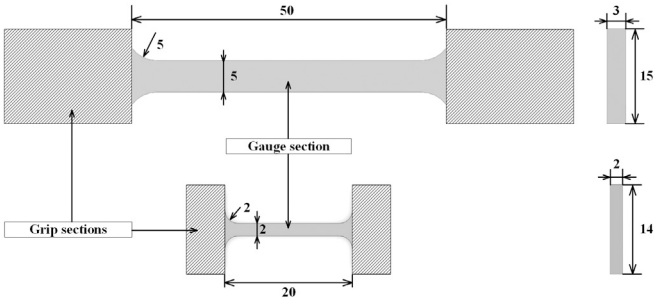

Fig. 1. The specimen sizes used for the uniaxial tension tests for low strain-rate case (top): 50 × 5 × 3 mm and high strain-rate case (below): 20 × 2 × 2 mm. The flat dumbbell shapes are chosen to avoid any fracture near the grips.

- to secure a tight grip, all the grip sections are glued to aluminium sheets before being mounted onto the testing machine,
- to prevent specimen fractures near the clamping positions, the transition regions are introduced with no significant influence on experimental results,
- to mitigate potential influences arising from radial constraints, the length–width ratio of 10:1 is chosen.

The preceding actions aim to mitigate the impact of different sample geometries on test results, especially at high strain rates. The temperature range of −20 °C to 60 °C is chosen similar to our previous study [36]. Note that for this material, the glass transition temperature (T_g) is measured to be the peak-temperature (8.8 °C) of the tan δ curve in the DMA experiment [36]. Additionally, 0.001/s to 500/s is chosen to investigate the strain-rate sensitivity.

The tensile experiments at low rates (0.001/s to 0.1/s) are performed using the Instron 5567 Universal Test Machine (see Fig. 2(a)) and the tests at high rates (10/s to 500/s) are conducted on the Instron VHS 40/50-20 Test Machine (see Fig. 2(b)). All experiments are performed in specially designed temperature chambers to ensure temperature stability. To show the robustness of the results, tests in different conditions are repeated three times to ensure the reproducibility. The gathered data is shown as the nominal stress (σ: force divided by the area of the initial cross-section of the specimen) and the nominal strain (ε: crosshead displacement divided by the original gauge length of the specimen). Note that more precise strain measurements could be achieved using techniques such as extensometers and Digital Image Correlation (DIC) techniques, based on deformation within the gauge section. However, these methods pose challenges when applied to high-speed conditions with finite deformations in a spatial-constrained temperature chamber. As an alternative approach, we have employed the clamping distance as a substitute for the gauge length. According to our pre-simulation, the use of transition regions does not lead to significant discrepancies in the stress results. Additionally, considering the discernible stress fluctuations observed during high-speed conditions, especially in the case of 500/s, the data smooth process is applied utilising the adjacent-averaging algorithm, which involves calculating the average value of successive data points and replacing them with their corresponding calculated average. By employing this algorithm, noise within the raw data was effectively mitigated, leading to improved clarity and visual representation of the results.

3. Results and discussions

3.1. Effects of temperature

The stress–strain results of tensile tests conducted at various temperatures are presented in Fig. 3 to show the effects of temperature variation on the stress of EPU. Based on Fig. 3, we find that the stresses under each strain level generally increase as the temperature decreases.

Table 1
Tangent moduli at 0.1/s under different temperatures.

Temperature [°C]	−20	0	20	60
Tangent modulus [MPa]	83.72 ± 16.95	33.83 ± 4.50	13.26 ± 1.52	8.98 ± 0.74

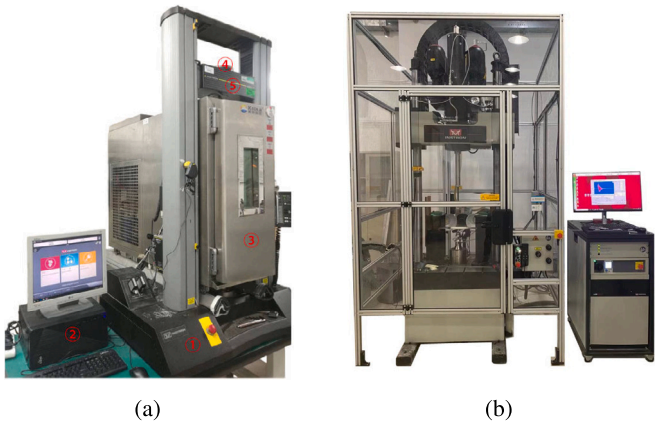

Fig. 2. (a) The structure of the Instron 5567 universal test machine used for our low-speed experiments [36]. It can reach the maximum tensile speed of 8 mm/s with the force measurement range from 0–500 N. (b) The structure of the Instron VHS 40/50-20 test machine used in our high-speed experiments. It has a top speed of 20 m/s equipped with a 0–5000 N force sensor. The frame rate ranges from 5000 fps to 10 000 fps.

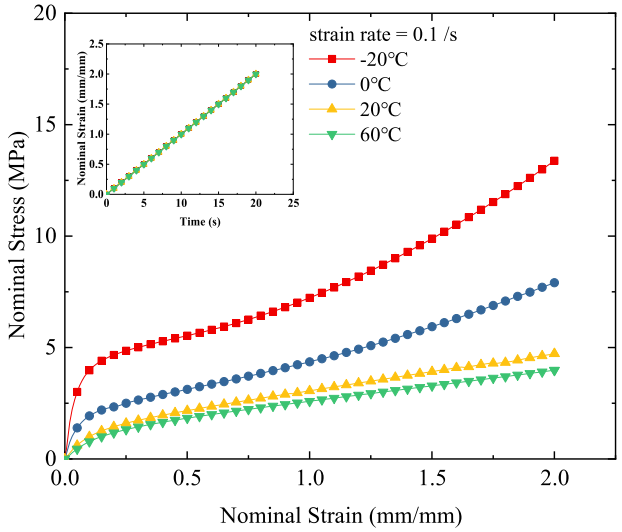

Fig. 3. Stress–strain curves of uniaxial tensile tests at 0.1/s under different temperatures with the inset depicting the strain controlling paths on the normal axis..

For example, at $\varepsilon = 2.0$, the stress at −20 °C is nearly 3.5 times greater than that at 60 °C. It should also be noted that the stresses show differences in the increasing trends with strain on either side of T_g (8.8 ° C). Table 1 lists the tangent moduli (slope of stress–strain curve from $\varepsilon = 0$ to $\varepsilon = 0.02$) variation with temperature. The modulus decreases more noticeably from −20 °C to 0 °C than that from 20 °C to 60 °C, indicating the rapid change in the viscosity (or relaxation time) across the glass transition [63].

To quantitatively investigate how the stress is sensitive to the temperature variation, we define a concept of "Thermal Sensitivity (S_T)":

$$S_T = \left|\frac{\partial \sigma}{\partial \Theta}\right|, \quad (1)$$

where Θ represents the absolute temperature. It provides insights into how stress changes with temperature and how these changes vary in

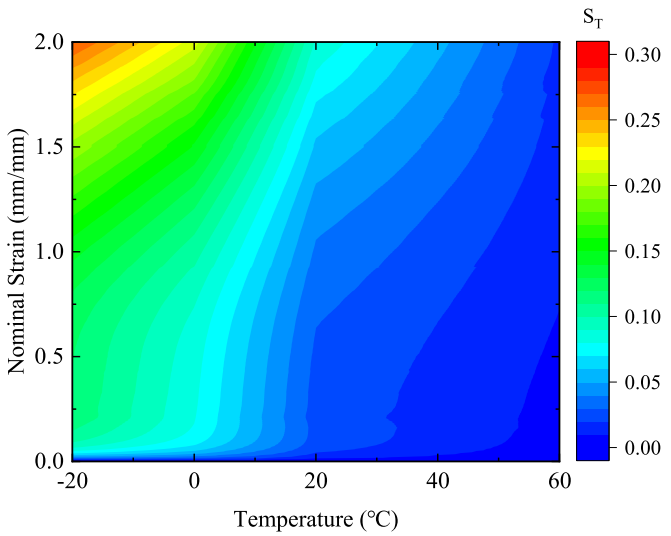

Fig. 4. The contour map of S_T as a function of nominal strain and temperature reflecting the thermal-sensitivity at the strain range from 0 to 2.0.

different regions, such as glassy state and rubbery state. The corresponding contour map as a coupled function of strain and temperature is plotted in Fig. 4. The contour displays a pronounced negative correlation trend, whereby the values of S_T increase as strain increases and temperature decreases. This suggests that the increase in the strain and the decrease in the temperature may have synergistic effects on S_T, suggesting a possible strain dependence of the thermal sensitivity [36].

The thermal sensitivity may be reasonably explained from a microscopic perspective. At a temperature lower than T_g, the energy of thermal molecular motion is low, and the chain segments are frozen in the system in a random form. That is to say, the polymer owns a solid-like shape but a liquid-like microstructure. At this state, chain segments are hard to unravel, preventing deformation propagation and resulting in a strong local stress response, i.e., becoming glassy. Therefore, the polymer in this situation has a much higher tangent modulus (see in Table 1). After temperature rises above T_g, the chain segment movement is activated and the polymer viscosity decreases dramatically resulting in flexibility of chain behaviour [63]. In this case, the polymer becomes rubbery, resulting in a lower modulus response. Moreover, the influence of strain level on the thermal sensitivity may be reasonably explained by continuous disentanglement of chain segments during stretching [64–67], resulting in an increasingly dominant influence on the kinematics of the soft polymer from temperature variations.

3.2. Effects of strain rate

The stress–strain results of tensile tests under different strain rates at 20 °C are presented in Fig. 5 to present the effects of strain-rate variation on the stress of EPU. It is important to note that, to the best of the authors' knowledge, capturing unloading behaviour within dynamic scenarios presents a challenge, and currently available equipment is limited in this regard. The stress–strain curves in Fig. 5 exhibit significant differences between the tests conducted at 0.001/s and 500/s, presenting the glass transition phenomenon of this soft polymer resulting from the increase in the strain rate. Based on Fig. 5, we find that the stresses under each strain level are positively related

Table 2
Tangent moduli under 20 °C at different strain rates.

Strain rate [/s]	0.001	0.01	0.1	10	100
Tangent modulus [MPa]	7.72 ± 0.80	10.22 ± 0.45	13.26 ± 1.52	27.69 ± 10.88	36.63 ± 12.80

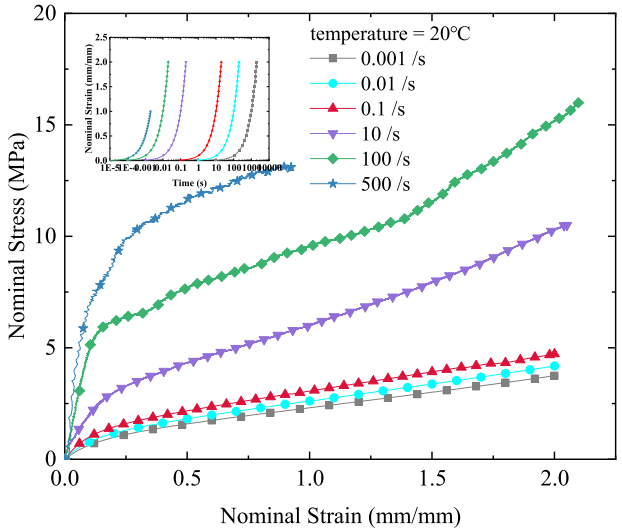

Fig. 5. Stress–strain curves of tensile tests at 20 °C under different rates. The inset depicts the strain-controlling paths with time on the logarithmic axis.

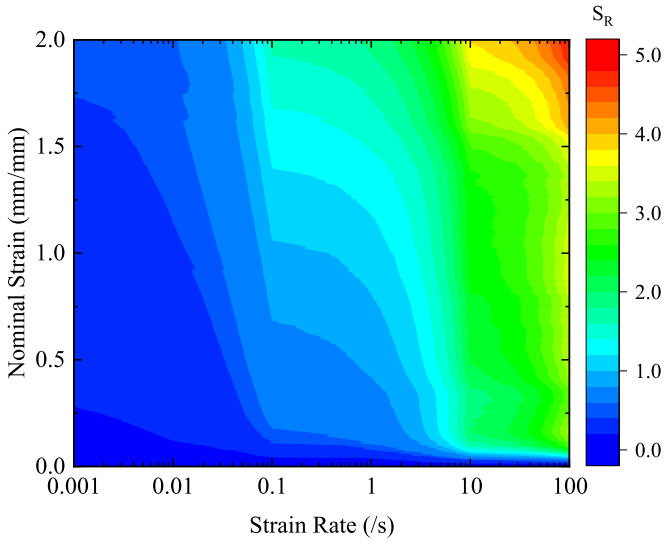

Fig. 6. The contour map of S_R as a function of nominal strain and strain rate reflecting the rate sensitivity extent at the strain range from 0 to 2.0.

to the strain rate. Tangent moduli at different strain rates are listed in Table 2, with the exception of the modulus at 500/s. This is because of the dramatic stress fluctuation at high strain rate conditions that makes it extremely difficult to accurately determine the corresponding modulus. Overall, the increase in the strain rate promotes stress in a manner similar to the temperature decrease effect.

Similar to S_T, a concept of "Rate Sensitivity (S_R)":

$$S_R = \left|\frac{\partial \sigma}{\partial \log \dot{\varepsilon}}\right|, \tag{2}$$

is defined, where $\dot{\varepsilon}$ denotes the strain rate and S_R gives an evaluation to see how the stress changes with the strain rate. The contour map of S_R as a coupled function of strain and strain rate is plotted in Fig. 6 in which S_R appears to exhibit a positive correlation with the strain and its rate. This contour suggests that the increases in the strain and the strain rate may have synergistic effects on S_R.

To facilitate discussion of subsequent microscale mechanisms, a rate transition point at the reference temperature (20 °C), $\dot{\varepsilon}_g$, is defined for convenience. At a strain rate lower than $\dot{\varepsilon}_g$, EPU behaves in a rubbery manner, while at a higher rate, it exhibits glassy behaviour. At high strain rates, within an extremely short period, chain segments must overcome higher intermolecular forces and energy barriers [68–71], which leads to an increase in the strain rate-sensitivity. As a result, chain mobility becomes restricted, leading to increased rigidity and viscosity, and hindering the deformation propagation. The entanglement network is likely to directly contribute to a greater stress, resulting in the increasing trend of tangent modulus with the increase in the strain rate. In contrast, the deformation propagation would be easier at low-rate cases since the entanglements have more time to unwind, rationalising the corresponding rubbery behaviours. Furthermore, the result of Fig. 6 indicates that the strain rate-sensitivity of the soft material may also be strain-dependent. Under large deformations, chain segments undergo extensive movement, and molecular slip may even occur (e.g., plastic deformation). Such significant changes in molecular internal structures and intermolecular forces compared with the initial state of the system may rationalise the influence of strain level on strain rate-sensitivity.

3.3. Coupled effects of temperature and strain rate

The aforementioned results fully state the thermal sensitivity and strain rate-sensitivity of this 3D-printed soft material, respectively. The coupled effect is then investigated by displaying the results under a wide domain of temperature-rate field in Fig. 7. At high temperatures, e.g., 60 °C (see Fig. 7(a)), EPU tends to undergo a transformation from the rubbery state to the glassy state with an increase in the strain rate. However, the curve corresponding to 500/s in the graph does not exhibit typical glass features, notably the presence of the apparent change of slope in the stress–strain curve. Note that such change is more discernible in the case of glassy materials, including but not limited to glass and ceramics. To investigate the effect of a further rate increase on the transition process, a loading condition with a strain rate of 1000/s (i.e., twice the previous highest value of 500/s) is carried out at this temperature. However, the corresponding curve does not significantly expedite the transformation, despite the higher strain rate. The situation is not the same for the low-temperature cases. For example, at −20 °C (see Fig. 7(d)), even for the low rate situation (0.1/s), the stress–strain starts to show strain softening near $\varepsilon = 0.15$. Upon the rate increase, this phenomenon becomes more obvious, which shows the differences compared to Fig. 7(a). From Figs. 7(a) to 7(d), it becomes evident that an increase in the applied strain rate leads to higher stress levels at each temperature. Notably, at lower temperatures, the magnitude of this stress increase demonstrates a more pronounced sensitivity to strain rate variations. This discernible trend highlights the interplay between temperature and strain rate on the mechanical behaviours of the EPU material.

Fig. 7 indicates comparable dependency between the temperature decrease and the rate increase to the mechanical properties of EPU. According to polymer physics, the molecular thermal motion has a similar relaxation process either over a short duration at high temperature or over a long period at low temperature [72]. This may be because of the changes in viscosity or relaxation time [63]. Therefore, at low temperatures, the reduction in thermal motion of molecules/atoms may hinder the chain segments from overcoming intermolecular forces and deforming, while at high strain rates, entanglements possibly have less

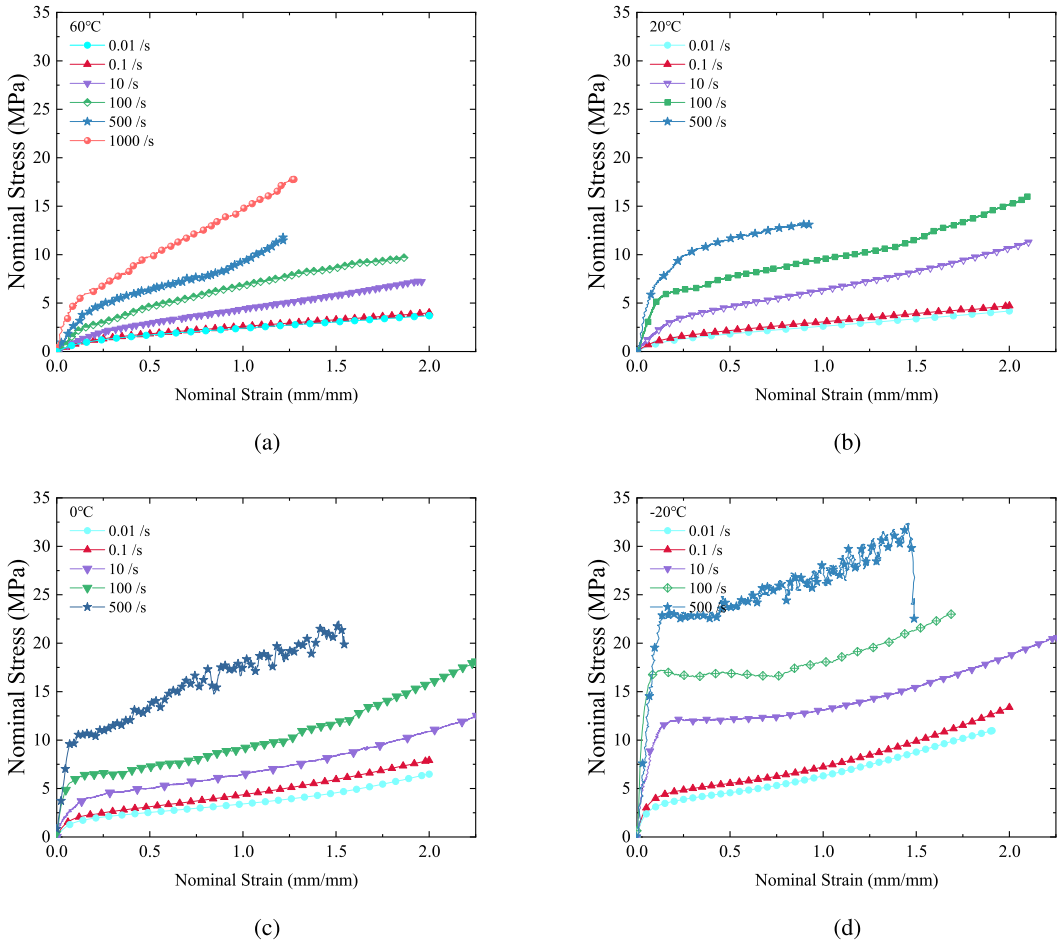

Fig. 7. Stress–strain curves of uniaxial tension under (a) 60 °C, (b) 20 °C, (c) 0 °C, and (d) −20 °C at different strain rates.

time to unwind resulting in a more challenging deformation propagation. These considerations rationalise the observed increase in the stiffness due to the decrease in temperature and/or the increase in the strain rate.

Furthermore, our experimental results adhere well to the classical Time–Temperature-Superposition (TTS) principle, which can be used in many aspects of viscoelasticity in polymer, including creep, stress relaxation, and dynamic mechanical analysis [32,72–75]. Ferry et al. [72] came up with the famous Williams–Landel–Ferry (WLF) equation as

$$\log\left(a_T\right) = -\frac{C_1\left[T - T_{ref}\right]}{C_2 + T - T_{ref}} \tag{3}$$

where T_{ref} is the reference temperature, and C_1, C_2 are WLF parameters. In this contribution, T_{ref} = 20 °C, C_1 = 20.62, C_2 = 224.20 °C. Tangent moduli at different temperatures and strain rates after the TTS modification are displayed in Fig. 8. All points essentially lie along an exponential growth line, which further indicates the synergistic effects of temperature decrease and strain-rate increase on mechanical behaviour (see Fig. 9).

Combined with Sections 3.1 and 3.2, we may probably assume that the strain level influences both thermal-sensitivity and strain rate-sensitivity. Upon deformation, segmental movements or even molecular slips occur within the system, and the entanglement is unravelled all the time. Alterations in the internal conformations of the molecules and intermolecular forces during deformation may rationalise the evolutions of S_T and S_R with strain shown in Figs. 4 and 6.

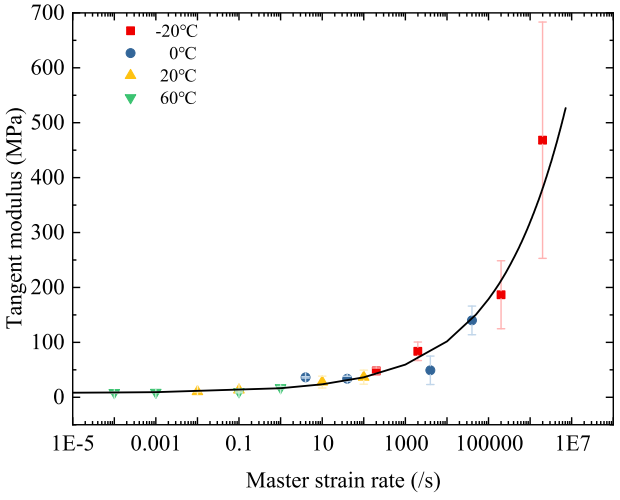

Fig. 8. The master curve of tangent modulus.

4. Conclusion

This study explores the thermo-mechanical properties of DLS-based EPU under strain rate and temperature conditions. A wide range of tensile tests is conducted spanning from −20 °C to 60 °C and 0.001/s

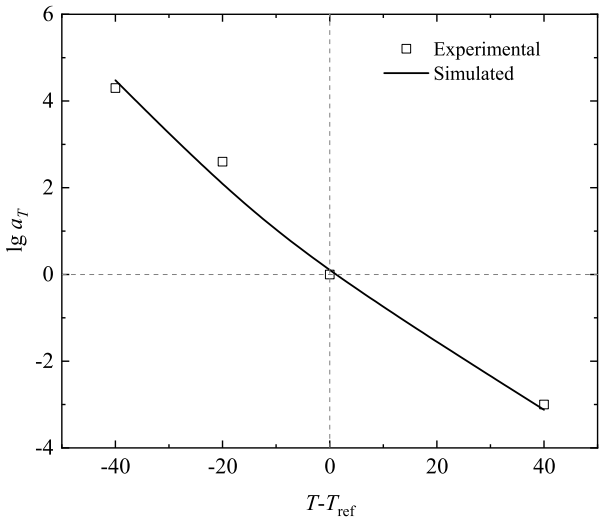

Fig. 9. The fitting result for a_T.

to 500/s. The results demonstrate that decreasing temperature and increasing strain rate elicit the elevation in the stress levels of EPU, and under specific conditions, such as −20 °C and 500/s, the occurrence of glass transition is observed. Furthermore, contour plots are presented to depict thermal and rate-sensitivities, i.e., the effects of temperature and strain rate variations on the stress response of the material. It is observed that as temperature decreases or strain rate increases, the stress becomes more susceptible with respect to changes in temperature or strain rate. The influences of strain level on these sensitivities are also discussed from the aspect of the variation in micro-conformation during deformation. Additionally, the TTS principle is used to further analyse the synergistic effects of temperature increase and strain rate increase. Overall, the present study offers significant insights into the performance alterations of 3D-printed EPU under varying temperature and strain rate conditions, enhancing the comprehension of material selection and structural optimisation for impact protective devices. Further research, such as fracture experiments and molecular dynamics simulations, is necessary to comprehensively examine the relationship between strength and strain rate, as well as the interrelationships between microstructures during deformation. This additional research may provide further insights into the glass transition phenomenon of 3D-printed soft polymers.

Declaration of competing interest

The authors declare that they have no known competing financial interests or personal relationships that could have appeared to influence the work reported in this paper.

Data availability

Data will be made available on request.

Acknowledgements

This research was funded by the National Science Fund for Distinguished Young Scholar (No. 11925203), the National Natural Science Foundation of China (No. 11672110), the Open Project Program of State Key Laboratory of Traction Power, China under Grant (No. TPL2003), and the financial support from the China Scholarship Council (CSC visiting PhD Fellowship No. 202206150100 to Jie Yang). M Hossain acknowledges the funding by the Swansea Bay City Deal and the European Regional Development Fund through the Welsh European Funding Office. This study is also supported by EPSRC, UK through the Supergen ORE Hub (EP/S000747/1), who have been awarded funding for the Flexible Fund project Submerged bi-axial fatigue analysis for flexible membrane Wave Energy Converters (FF2021-1036). M Hossain also acknowledges the support of the Royal Society through the International Exchange Grant (IEC/NSFC/211316) with the National Natural Science Foundation of China (NSFC).

References

[1] S.C. Ligon, R. Liska, J. Stampfl, M. Gurr, R. Mülhaupt, Polymers for 3D printing and customized additive manufacturing, Chem. Rev. 117 (15) (2017) 10212–10290, http://dx.doi.org/10.1021/acs.chemrev.7b00074, URL https://pubs.acs.org/doi/10.1021/acs.chemrev.7b00074.

[2] J.W. Stansbury, M.J. Idacavage, 3D printing with polymers: challenges among expanding options and opportunities, Dent. Mater. 32 (1) (2016) 54–64, http://dx.doi.org/10.1016/j.dental.2015.09.018, URL https://linkinghub.elsevier.com/retrieve/pii/S0109564115004145.

[3] J.F. Christ, N. Aliheidari, A. Ameli, P. Pötschke, 3D printed highly elastic strain sensors of multiwalled carbon nanotube/Thermoplastic polyurethane nanocomposites, Mater. Des. 131 (2017) 394–401, http://dx.doi.org/10.1016/j.matdes.2017.06.011, URL https://linkinghub.elsevier.com/retrieve/pii/S0264127517305944.

[4] J. Christ, N. Aliheidari, P. Pötschke, A. Ameli, Bidirectional and stretchable piezoresistive sensors enabled by multimaterial 3D printing of carbon nanotube/Thermoplastic Polyurethane Nanocomposites, Polymers 11 (1) (2018) 11, http://dx.doi.org/10.3390/polym11010011, URL http://www.mdpi.com/2073-4360/11/1/11.

[5] V. Slesarenko, S. Rudykh, Towards mechanical characterization of soft digital materials for multimaterial 3D-printing, Internat. J. Engrg. Sci. 123 (2018) 62–72, http://dx.doi.org/10.1016/j.ijengsci.2017.11.011, URL https://linkinghub.elsevier.com/retrieve/pii/S0020722517306262.

[6] A. Unkovskiy, S. Spintzyk, J. Brom, F. Huettig, C. Keutel, Direct 3D printing of silicone facial prostheses: A preliminary experience in digital workflow, J. Prosthet. Dent. 120 (2) (2018) 303–308, http://dx.doi.org/10.1016/j.prosdent.2017.11.007, arXiv:29429837. URL https://linkinghub.elsevier.com/retrieve/pii/S0022391317307795.

[7] M.Y. Khalid, Z.U. Arif, R. Noroozi, M. Hossain, S. Ramakrishna, R. Umer, 3D/4D printing of cellulose nanocrystals-based biomaterials: additives for sustainable applications, Int. J. Biol. Macromol. 251 (2023) 126287, http://dx.doi.org/10.1016/j.ijbiomac.2023.126287, URL https://linkinghub.elsevier.com/retrieve/pii/S0141813023031835.

[8] Z.U. Arif, M.Y. Khalid, R. Noroozi, M. Hossain, H.H. Shi, A. Tariq, S. Ramakrishna, R. Umer, Additive manufacturing of sustainable biomaterials for biomedical applications, Asian J. Pharm. Sci. 18 (3) (2023) 100812, http://dx.doi.org/10.1016/j.ajps.2023.100812, URL https://linkinghub.elsevier.com/retrieve/pii/S1818087623000399.

[9] A. Tariq, Z.U. Arif, M.Y. Khalid, M. Hossain, P.I. Rasool, R. Umer, S. Ramakrishna, Recent advances in the additive manufacturing of stimuli-responsive soft polymers, Adv. Eng. Mater. (2023) 2301074, http://dx.doi.org/10.1002/adem.202301074, URL https://onlinelibrary.wiley.com/doi/10.1002/adem.202301074.

[10] R. Zhang, W. Huang, P. Lyu, S. Yan, X. Wang, J. Ju, Polyurea for blast and impact protection: a review, Polymers 14 (13) (2022) 2670, http://dx.doi.org/10.3390/polym14132670, URL https://www.mdpi.com/2073-4360/14/13/2670.

[11] O. Grimaldo Ruiz, M. Rodriguez Reinoso, E. Ingrassia, F. Vecchio, F. Maniero, V. Burgio, M. Civera, I. Bitan, G. Lacidogna, C. Surace, Design and mechanical characterization using digital image correlation of soft tissue-mimicking polymers, Polymers 14 (13) (2022) 2639, http://dx.doi.org/10.3390/polym14132639, URL https://www.mdpi.com/2073-4360/14/13/2639.

[12] T. Hanuhov, N. Cohen, Thermally induced deformations in multi-layered polymeric struts, Int. J. Mech. Sci. 215 (2022) 106959, http://dx.doi.org/10.1016/j.ijmecsci.2021.106959, URL https://linkinghub.elsevier.com/retrieve/pii/S002074032100669X.

[13] B. John, R. van Wim, L. Charles, H. Mark, T. Ryan, K. Arda, L. Jennifer, M. Lakshminarayanan, Shape-shifting structured lattices via multimaterial 4D printing, Proc. Natl. Acad. Sci. 116 (42) (2019) 20856–20862, http://dx.doi.org/10.1073/pnas.1908806116, URL https://pnas.org/doi/full/10.1073/pnas.1908806116.

[14] J. Wu, C. Yuan, Z. Ding, M. Isakov, Y. Mao, T. Wang, M.L. Dunn, H.J. Qi, Multi-shape active composites by 3D printing of digital shape memory polymers, Sci. Rep. 6 (1) (2016) 24224, http://dx.doi.org/10.1038/srep24224, URL https://www.nature.com/articles/srep24224.

[15] Y. Zhang, M.-T. Hsieh, L. Valdevit, Mechanical performance of 3D printed interpenetrating phase composites with spinodal topologies, Compos. Struct. 263 (2021) http://dx.doi.org/10.1016/j.compstruct.2021.113693.

[16] A. Georgopoulou, T. Sebastian, F. Clemens, Thermoplastic elastomer composite filaments for strain sensing applications extruded with a fused deposition modelling 3D printer, Flex. Print. Electron. 5 (3) (2020) http://dx.doi.org/10.1088/2058-8585/ab9a22.

[17] G.X. Gu, M. Takaffoli, A.J. Hsieh, M.J. Buehler, Biomimetic additive manufactured polymer composites for improved impact resistance, Extrem. Mech. Lett. 9 (2016) 317–323, http://dx.doi.org/10.1016/j.eml.2016.09.006.

[18] H.M. Lee, J. Sung, B. Ko, H. Lee, S. Park, H. So, G.H. Yoon, Modeling and application of anisotropic hyperelasticity of PDMS polymers with surface patterns obtained by additive manufacturing technology, J. Mech. Behav. Biomed. Mater. 118 (2021) 104412, http://dx.doi.org/10.1016/j.jmbbm.2021.104412, URL https://linkinghub.elsevier.com/retrieve/pii/S1751616121001004.

[19] Y. Xiang, C. Schilling, N. Arora, A. Boydston, S. Rudykh, Mechanical characterization and constitutive modeling of visco-hyperelasticity of photocured polymers, Addit. Manuf. 36 (2020) 101511, http://dx.doi.org/10.1016/j.addma.2020.101511, URL https://linkinghub.elsevier.com/retrieve/pii/S2214860420308836.

[20] K. Yu, A. Xin, Q. Wang, Mechanics of light-activated self-healing polymer networks, J. Mech. Phys. Solids 124 (2019) 643–662, http://dx.doi.org/10.1016/j.jmps.2018.11.019, URL https://linkinghub.elsevier.com/retrieve/pii/S0022509618308123.

[21] Z. Zhao, X. Mu, N. Sowan, Y. Pei, C.N. Bowman, H. Jerry Qi, D. Fang, Effects of oxygen on light activation in covalent adaptable network polymers, Soft Matter 11 (30) (2015) 6134–6144, http://dx.doi.org/10.1039/C5SM00555H, URL http://xlink.rsc.org/?DOI=C5SM00555H.

[22] Y.C. Kim, S. Hong, H. Sun, M.G. Kim, K. Choi, J. Cho, H.R. Choi, J.C. Koo, H. Moon, D. Byun, K.J. Kim, J. Suhr, S.H. Kim, J.-D. Nam, UV-curing kinetics and performance development of in situ curable 3D printing materials, Eur. Polym. J. 93 (2017) 140–147, http://dx.doi.org/10.1016/j.eurpolymj.2017.05.041, URL https://linkinghub.elsevier.com/retrieve/pii/S0014305717303348.

[23] A. Vyas, V. Garg, S.B. Ghosh, S. Bandyopadhyay-Ghosh, Photopolymerizable resin-based 3D printed biomedical composites: Factors affecting resin viscosity, Vol. 62 (2022) 1435–1439. http://dx.doi.org/10.1016/j.matpr.2022.01.172.

[24] Y. Zhou, F. Wang, Z. Yang, X. Hu, Y. Pan, Y. Lu, M. Jiang, 3D printing of polyurethane/Nanocellulose shape memory composites with tunable glass transition temperature, Ind. Crops Prod 182 (2022) 114831, http://dx.doi.org/10.1016/j.indcrop.2022.114831, URL https://linkinghub.elsevier.com/retrieve/pii/S0926669022003144.

[25] X. Lin, J. Gao, J. Wang, R. Wang, M. Gong, L. Zhang, Y. Lu, D. Wang, L. Zhang, Desktop printing of 3D thermoplastic polyurethane parts with enhanced mechanical performance using filaments with varying stiffness, Addit. Manuf. 47 (2021) http://dx.doi.org/10.1016/j.addma.2021.102267.

[26] X. Lin, P. Coates, M. Hebda, R. Wang, Y. Lu, L. Zhang, Experimental analysis of the tensile property of FFF-printed elastomers, Polym. Test. 90 (2020) 106687, http://dx.doi.org/10.1016/j.polymertesting.2020.106687, URL https://linkinghub.elsevier.com/retrieve/pii/S0142941820303305.

[27] Z.S. Petrović, J. Ferguson, Polyurethane elastomers, Prog. Polym. Sci. 16 (5) (1991) 695–836, http://dx.doi.org/10.1016/0079-6700(91)90011-9, URL https://linkinghub.elsevier.com/retrieve/pii/0079670091900119.

[28] D. Chattopadhyay, K. Raju, Structural engineering of polyurethane coatings for high performance applications, Prog. Polym. Sci. 32 (3) (2007) 352–418, http://dx.doi.org/10.1016/j.progpolymsci.2006.05.003, URL https://linkinghub.elsevier.com/retrieve/pii/S0079670006001365.

[29] P. Krol, Synthesis methods, chemical structures and phase structures of linear polyurethanes. properties and applications of linear polyurethanes in polyurethane elastomers, copolymers and ionomers, Prog. Mater. Sci. 52 (6) (2007) 915–1015, http://dx.doi.org/10.1016/j.pmatsci.2006.11.001, URL https://linkinghub.elsevier.com/retrieve/pii/S007964250600079X.

[30] L. Xue, W. Mock, T. Belytschko, Penetration of DH-36 steel plates with and without polyurea coating, Mech. Mater. 42 (11) (2010) 981–1003, http://dx.doi.org/10.1016/j.mechmat.2010.08.004, URL https://linkinghub.elsevier.com/retrieve/pii/S0167663610001110.

[31] J.O. Akindoyo, M.D.H. Beg, S. Ghazali, M.R. Islam, N. Jeyaratnam, A.R. Yuvaraj, Polyurethane types, synthesis and applications – a review, RSC Adv. 6 (115) (2016) 114453–114482, http://dx.doi.org/10.1039/C6RA14525F, URL http://xlink.rsc.org/?DOI=C6RA14525F.

[32] Z. Liao, X. Yao, L. Zhang, M. Hossain, J. Wang, S. Zang, Temperature and strain rate dependent large tensile deformation and tensile failure behavior of transparent polyurethane at intermediate strain rates, Int. J. Impact Eng. 129 (2019) 152–167, http://dx.doi.org/10.1016/j.ijimpeng.2019.03.005, URL https://linkinghub.elsevier.com/retrieve/pii/S0734743X18304937.

[33] M. Nikoukalam, P. Sideris, Experimental characterization and constitutive modeling of polyurethanes for structural applications, accounting for damage, hysteresis, loading rate and long term effects, Eng. Struct. 198 (2019) 109462, http://dx.doi.org/10.1016/j.engstruct.2019.109462, URL https://linkinghub.elsevier.com/retrieve/pii/S0141029618333157.

[34] L. Cheng, J. Shao, F. Wang, Z. Li, F. Dai, Strain rate dependent mechanical behavior of b. Mori silk, a. assama silk, a. Pernyi silk and a. Ventricosus spider silk, Mater. Des. 195 (2020) 108988, http://dx.doi.org/10.1016/j.matdes.2020.108988, URL https://linkinghub.elsevier.com/retrieve/pii/S0264127520305220.

[35] J. Cui, Y. Shi, X. Zhang, W. Huang, M. Ma, Experimental study on the tension and puncture behavior of spray polyurea at high strain rates, Polym. Test. 93 (2021) 106863, http://dx.doi.org/10.1016/j.polymertesting.2020.106863, URL https://linkinghub.elsevier.com/retrieve/pii/S0142941820320924.

[36] J. Yang, Z. Liao, M. Hossain, G. Huang, X. Zhou, F. Liu, A.S. Alzaidi, X. Yao, Thermo-mechanical properties of digitally-printed elastomeric polyurethane: experimental characterisation and constitutive modelling using a nonlinear temperature-strain coupled scaling strategy, Int. J. Solids Struct. 267 (2023) 112163, http://dx.doi.org/10.1016/j.ijsolstr.2023.112163, URL https://linkinghub.elsevier.com/retrieve/pii/S0020768323000604.

[37] H. Qi, M. Boyce, Stress–strain behavior of thermoplastic polyurethanes, Mech. Mater. 37 (8) (2005) 817–839, http://dx.doi.org/10.1016/j.mechmat.2004.08.001, URL https://linkinghub.elsevier.com/retrieve/pii/S0167663604001140.

[38] H. Qi, Constitutive model for stretch-induced softening of the stress-stretch behavior of elastomeric materials, J. Mech. Phys. Solids 52 (10) (2004) 2187–2205, http://dx.doi.org/10.1016/j.jmps.2004.04.008, URL https://linkinghub.elsevier.com/retrieve/pii/S0022509604000845.

[39] A.V. Amirkhizi, J. Isaacs, J. McGee, S. Nemat-Nasser, An experimentally-based viscoelastic constitutive model for polyurea, including pressure and temperature effects, Phil. Mag. 86 (36) (2006) 5847–5866, http://dx.doi.org/10.1080/14786430600833198, URL https://www.tandfonline.com/doi/full/10.1080/14786430600833198.

[40] J. Yi, M. Boyce, G. Lee, E. Balizer, Large deformation rate-dependent stress–strain behavior of polyurea and polyurethanes, Polymer 47 (1) (2006) 319–329, http://dx.doi.org/10.1016/j.polymer.2005.10.107, URL https://linkinghub.elsevier.com/retrieve/pii/S0032386105015740.

[41] O.A. Shergold, N.A. Fleck, D. Radford, The uniaxial stress versus strain response of pig skin and silicone rubber at low and high strain rates, Int. J. Impact Eng. 32 (9) (2006) 1384–1402, http://dx.doi.org/10.1016/j.ijimpeng.2004.11.010, URL https://linkinghub.elsevier.com/retrieve/pii/S0734743X04002325.

[42] S.S. Sarva, S. Deschanel, M.C. Boyce, W. Chen, Stress–strain behavior of a polyurea and a polyurethane from low to high strain rates, Polymer 48 (8) (2007) 2208–2213, http://dx.doi.org/10.1016/j.polymer.2007.02.058, URL https://linkinghub.elsevier.com/retrieve/pii/S0032386107002121.

[43] J. Shim, D. Mohr, Using split Hopkinson pressure bars to perform large strain compression tests on polyurea at low, intermediate and high strain rates, Int. J. Impact Eng. 36 (9) (2009) 1116–1127, http://dx.doi.org/10.1016/j.ijimpeng.2008.12.010, URL https://linkinghub.elsevier.com/retrieve/pii/S0734743X0800328X.

[44] L. Zhang, X. Yao, S. Zang, Y. Gu, Temperature- and strain rate-dependent constitutive modeling of the large deformation behavior of a transparent polyurethane interlayer, Polym. Eng. Sci. 55 (8) (2015) 1864–1872, http://dx.doi.org/10.1002/pen.24026, URL https://onlinelibrary.wiley.com/doi/10.1002/pen.24026.

[45] X. Chen, J. Lai, X.-l. Chang, Y. Zhang, L. Zhang, C. Wang, Compressive mechanical properties of HTPB propellant at low temperatures and high strain rates, Results Phys. 7 (2017) 4079–4084, http://dx.doi.org/10.1016/j.rinp.2017.10.034, URL https://linkinghub.elsevier.com/retrieve/pii/S2211379717312846.

[46] H. Chen, A. Trivedi, C. Siviour, Application of linear viscoelastic continuum damage theory to the low and high strain rate response of thermoplastic polyurethane, Exp. Mech. 60 (7) (2020) 925–936, http://dx.doi.org/10.1007/s11340-020-00608-2, URL https://link.springer.com/10.1007/s11340-020-00608-2.

[47] C. Gong, Y. Chen, T. Li, Z. Liu, Z. Zhuang, B. Guo, H. Wang, L. Dai, Free volume based nonlinear viscoelastic model for polyurea over a wide range of strain rates and temperatures, Mech. Mater. 152 (2021) 103650, http://dx.doi.org/10.1016/j.mechmat.2020.103650, URL https://linkinghub.elsevier.com/retrieve/pii/S0167663620306852.

[48] B. Shamsadinlo, M.R. Sheikhi, O. Unver, B. Yildirim, Numerical and empirical modeling of peak deceleration and stress analysis of polyurethane elastomer under impact loading test, Polym. Test. 89 (2020) 106594, http://dx.doi.org/10.1016/j.polymertesting.2020.106594, URL https://linkinghub.elsevier.com/retrieve/pii/S0142941820304451.

[49] H. Guo, W. Guo, A.V. Amirkhizi, R. Zou, K. Yuan, Experimental investigation and modeling of mechanical behaviors of polyurea over wide ranges of strain rates and temperatures, Polym. Test. 53 (2016) 234–244, http://dx.doi.org/10.1016/j.polymertesting.2016.06.004, URL https://linkinghub.elsevier.com/retrieve/pii/S0142941816302938.

[50] H. Guo, W. Guo, A.V. Amirkhizi, Constitutive modeling of the tensile and compressive deformation behavior of polyurea over a wide range of strain rates, Constr. Build. Mater. 150 (2017) 851–859, http://dx.doi.org/10.1016/j.conbuildmat.2017.06.055, URL https://linkinghub.elsevier.com/retrieve/pii/S0950061817311959.

[51] L. Zhang, X. Yao, S. Zang, Y. Gu, Temperature- and strain rate-dependent constitutive modeling of the large deformation behavior of a transparent polyurethane interlayer, Polym. Eng. Sci. 55 (8) (2015) 1864–1872, http://dx.doi.org/10.1002/pen.24026, URL https://onlinelibrary.wiley.com/doi/10.1002/pen.24026.

[52] J. Yi, M. Boyce, G. Lee, E. Balizer, Large deformation rate-dependent stress–strain behavior of polyurea and polyurethanes, Polymer 47 (1) (2006) 319–329, http://dx.doi.org/10.1016/j.polymer.2005.10.107, URL https://linkinghub.elsevier.com/retrieve/pii/S0032386105015740.

[53] S.S. Sarva, S. Deschanel, M.C. Boyce, W. Chen, Stress–strain behavior of a polyurea and a polyurethane from low to high strain rates, Polymer 48 (8) (2007) 2208–2213, http://dx.doi.org/10.1016/j.polymer.2007.02.058, URL https://linkinghub.elsevier.com/retrieve/pii/S0032386107002121.

[54] H. Guo, W. Guo, A.V. Amirkhizi, R. Zou, K. Yuan, Experimental investigation and modeling of mechanical behaviors of polyurea over wide ranges of strain rates and temperatures, Polym. Test. 53 (2016) 234–244, http://dx.doi.org/10.1016/j.polymertesting.2016.06.004, URL https://linkinghub.elsevier.com/retrieve/pii/S0142941816302938.

[55] M.L. Williams, R.F. Landel, J.D. Ferry, The temperature dependence of relaxation mechanisms in amorphous polymers and other glass-forming liquids, J. Am. Chem. Soc. 77 (14) (1955) 3701–3707, http://dx.doi.org/10.1021/ja01619a008, URL https://pubs.acs.org/doi/abs/10.1021/ja01619a008.

[56] X. Zhang, H. Hao, Y. Shi, J. Cui, The mechanical properties of polyvinyl butyral (PVB) at high strain rates, Constr. Build. Mater. 93 (2015) 404–415, http://dx.doi.org/10.1016/j.conbuildmat.2015.04.057, URL https://linkinghub.elsevier.com/retrieve/pii/S0950061815006649.

[57] Y. Liu, L. Wang, Multiobjective-clustering-based optimal heterogeneous sensor placement method for thermo-mechanical load identification, Int. J. Mech. Sci. 253 (2023) 108369, http://dx.doi.org/10.1016/j.ijmecsci.2023.108369, URL https://linkinghub.elsevier.com/retrieve/pii/S0020740323002710.

[58] M. Hossain, R. Navaratne, D. Perić, 3D printed elastomeric polyurethane: viscoelastic experimental characterizations and constitutive modelling with non-linear viscosity functions, Int. J. Non-Linear Mech. 126 (2020) 103546, http://dx.doi.org/10.1016/j.ijnonlinmec.2020.103546, URL https://linkinghub.elsevier.com/retrieve/pii/S0020746220302080.

[59] M. Hossain, Z. Liao, An additively manufactured silicone polymer: thermo-viscoelastic experimental study and computational modelling, Addit. Manuf. 35 (2020) 101395, http://dx.doi.org/10.1016/j.addma.2020.101395, URL https://linkinghub.elsevier.com/retrieve/pii/S2214860420307673.

[60] J.R. Tumbleston, D. Shirvanyants, N. Ermoshkin, R. Janusziewicz, A.R. Johnson, D. Kelly, K. Chen, R. Pinschmidt, J.P. Rolland, A. Ermoshkin, E.T. Samulski, J.M. DeSimone, Continuous liquid interface production of 3D objects, Science 347 (6228) (2015) 1349–1352, http://dx.doi.org/10.1126/science.aaa2397, URL https://www.science.org/doi/10.1126/science.aaa2397.

[61] M. Pagac, D. Schwarz, J. Petru, S. Polzer, 3D printed polyurethane exhibits isotropic elastic behavior despite its anisotropic surface, Rapid Prototyp. J. 26 (8) (2020) 1371–1378, http://dx.doi.org/10.1108/RPJ-02-2019-0027, URL https://www.emerald.com/insight/content/doi/10.1108/RPJ-02-2019-0027/full/html.

[62] F. Cosmi, A. Dal Maso, A mechanical characterization of SLA 3D-printed specimens for low-budget applications, Mater. Today: Proc. 32 (2020) 194–201, http://dx.doi.org/10.1016/j.matpr.2020.04.602, URL https://linkinghub.elsevier.com/retrieve/pii/S2214785320332247.

[63] J.H. Gibbs, E.A. DiMarzio, Nature of the glass transition and the glassy state, J. Chem. Phys. 28 (3) (1958) 373–383, http://dx.doi.org/10.1063/1.1744141, URL http://aip.scitation.org/doi/10.1063/1.1744141.

[64] T. Zheng, S.K. Wang, L. Zhou, X. Li, H.C. Zhang, The disentanglement and shear properties of amorphous polyethylene during friction: insights from molecular dynamics simulations, Appl. Surf. Sci. 580 (2022) http://dx.doi.org/10.1016/j.apsusc.2021.152301.

[65] A. Moyassari, T. Gkourmpis, M.S. Hedenqvist, U.W. Gedde, Molecular dynamics simulations of short-chain branched bimodal polyethylene: topological characteristics and mechanical behavior, Macromolecules 52 (3) (2019) 807–818, http://dx.doi.org/10.1021/acs.macromol.8b01874.

[66] C. Ma, T. Ji, C.G. Robertson, R. Rajeshbabu, J. Zhu, Y. Dong, Molecular insight into the mullins effect: irreversible disentanglement of polymer chains revealed by molecular dynamics simulations, Phys. Chem. Chem. Phys. 19 (29) (2017) 19468–19477, http://dx.doi.org/10.1039/C7CP01142C.

[67] C. Teng, Y. Gao, X.L. Wang, W. Jiang, C. Zhang, R. Wang, D.S. Zhou, G. Xue, Reentanglement kinetics of freeze-dried polymers above the glass transition temperature, Macromolecules 45 (16) (2012) 6648–6651, http://dx.doi.org/10.1021/ma300885w.

[68] M.V.T. daCosta, E.K. Gamstedt, Energy-release rates and opening of cracks in thin barrier coatings on polymer substrates subjected to tensile loading, Eng. Fract. Mech. 235 (2020) http://dx.doi.org/10.1016/j.engfracmech.2020.107151.

[69] P. Golewski, A. Rusinek, T. Sadowski, Material characterization of PMC/TBC Composite Under High Strain Rates and elevated temperatures, Materials 13 (1) (2020) http://dx.doi.org/10.3390/ma13010167.

[70] S. Bell, E.M. Terentjev, Unfolding of globular polymers by external force, J. Chem. Phys. 143 (18) (2015) http://dx.doi.org/10.1063/1.4935393.

[71] A.G. Hati, F.L. Aachmann, B.T. Stokke, G. Skjak-Braek, M. Sletmoen, Energy landscape of alginate-epimerase interactions assessed by optical tweezers and atomic force microscopy, PLOS ONE 10 (10) (2015) http://dx.doi.org/10.1371/journal.pone.0141237.

[72] J.D. Ferry, Viscoelastic Properties of Polymers, John Wiley & Sons, 1980.

[73] L.W. Morland, E. Lee, Stress analysis for linear viscoelastic materials with temperature variation, Trans. Soc. Rheol. 4 (1) (1960) 233–263, http://dx.doi.org/10.1122/1.548856.

[74] R. Muki, E. Sternberg, On transient thermal stresses in viscoelastic materials with temperature-dependent properties, 1961, http://dx.doi.org/10.1115/1.3641651.

[75] Z. Liao, M. Hossain, X. Yao, M. Mehnert, P. Steinmann, On thermo-viscoelastic experimental characterization and numerical modelling of VHB polymer, Int. J. Non-Linear Mech. 118 (2020) 103263, http://dx.doi.org/10.1016/j.ijnonlinmec.2019.103263, URL https://linkinghub.elsevier.com/retrieve/pii/S0020746219303415.